Supplementary Material

Two-dimensional nitrogen and phosphorus co-doped mesoporous carbon-graphene nanosheets anode for high-performance potassium-ion capacitor

Tong Li[1,#], Xinli Huang[1,#], Shulai Lei[2,3,#], Jing Zhang[4,*], Xin Li[1], Chengxiang Wang[1], Zhiwei Zhang[1], Shijie Wang[5,*], Longwei Yin[1], Rutao Wang[1,*]

[1]Key Laboratory for Liquid-Solid Structural Evolution and Processing of Materials, Ministry of Education, School of Materials Science and Engineering, Shandong University, Jinan 250061, Shandong, China.
[2]Hubei Key Laboratory of Low Dimensional Optoelectronic Materials and Devices, Hubei University of Arts and Science, Xiangyang 441053, Hubei, China.
[3]Institute of Chemistry, Free University of Berlin, Arnimallee 22, Berlin D-14195, Germany.
[4]Shandong Key Laboratory for Special Silicon-Containing Material, Advanced Materials Institute, Qilu University of Technology (Shandong Academy of Sciences), Jinan 250014, Shandong, China.
[5]Shanghai Institute of Ceramics, Chinese Academy of Sciences, Shanghai 200050, China.
[#]These authors contributed equally to this work.

ADDITIONAL EXPERIMENTAL

Electrochemical Measurements

Electrochemical workstation (CHI760E, Shanghai Chenghua, Ltd., China) was used to record cyclic voltammetry curves (CV), galvanostatic charge/discharge curves and electrical impedance spectroscopy (EIS). A battery test system (Land CT2001A model, Wuhan Land Electronics, Ltd., China) was used to implement rate life-span tests and galvanostatic intermittent titration technique (GITT) test for half-cell and hybrid cells.

The energy density (E, Wh kg^{-1}) of PICs can be evaluated by the constant discharge current (I), the cell voltage (V) and the start and end of-discharge time (t_1 and t_2) according to the following equation:

$$E = \int_{t_1}^{t_2} IV \, dt \quad (1)$$

The power density (P, W kg^{-1}) of PICs can be evaluated by the energy density (E) and the discharging time (t) according to the following equation:

$$P = E/t \quad (2)$$

Density Functional Theory (DFT) computational details

All the first-principles calculations are performed using the density functional theory (DFT), as implemented in Vienna ab initio Simulation Package (VASP). The interactions between electrons and ion-cores are described by the projector augmented wave (PAW) method and the exchange-correlation interactions are treated by the generalized gradient approximation (GGA) in the form proposed by Perdew, Burke, and Ernzerhof (PBE). The cut-off energy is set to 500 eV for the plane-wave basis in all our calculations. Γ-centered k-point meshes of 3 × 3 × 1 based on Monkhorst-Pack scheme are employed for the geometric structure's calculations. A vacuum space of 15.0 Å along the z-axis is adopted to ensure no appreciable interaction between the image layers under periodic boundary condition. The self-consistent convergence criterion for the total energy and Hellmann-Feynman force are smaller than 10^{-5} eV and 0.01 eV/Å, respectively.

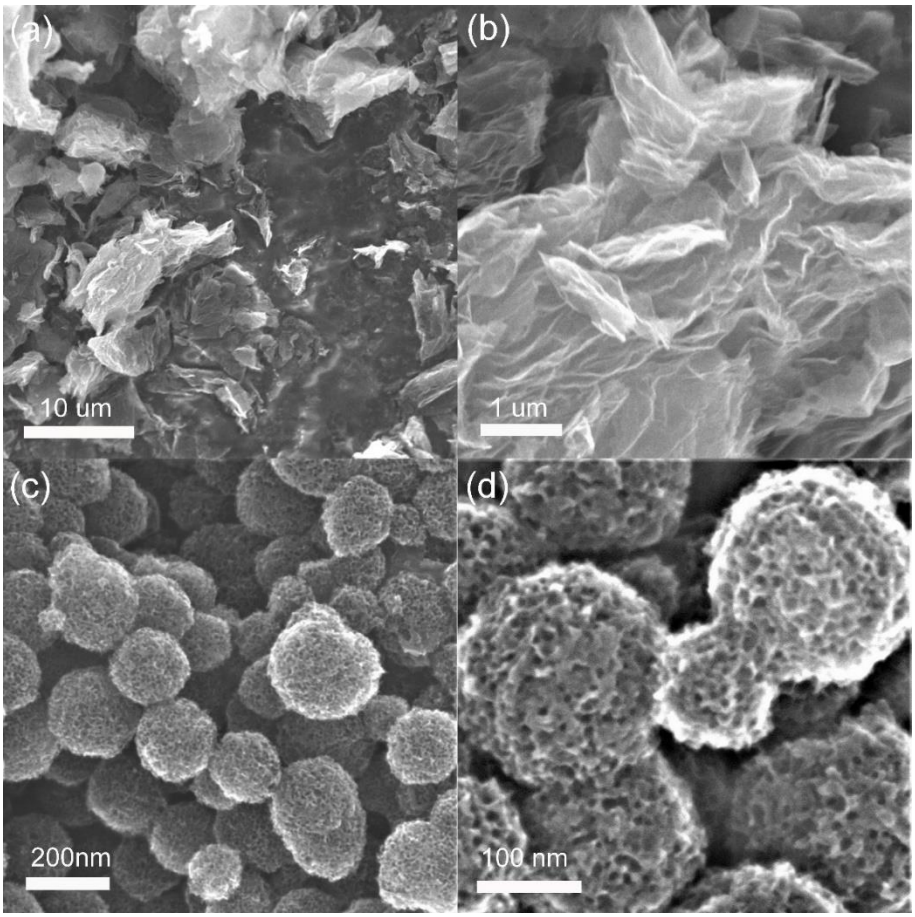

Supplementary Figure 1. SEM images of (a, b) RGO and (c, d) N/P-MC.

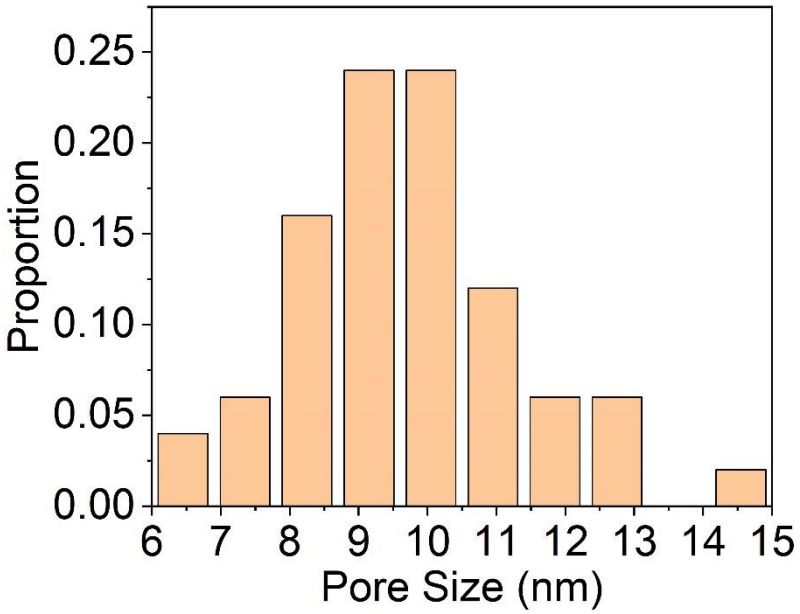

Supplementary Figure 2. Pore size distribution evaluated from TEM image of Fig. 1f.

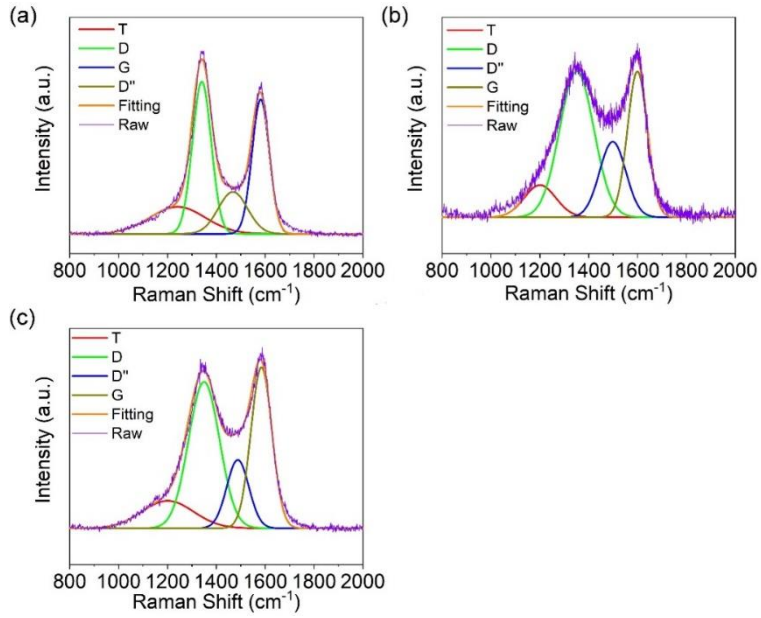

Supplementary Figure 3. Fitted Raman spectra curves of as-prepared (a) RGO, (b) N/P-MC, and (c) N/P-MC@RGO samples.

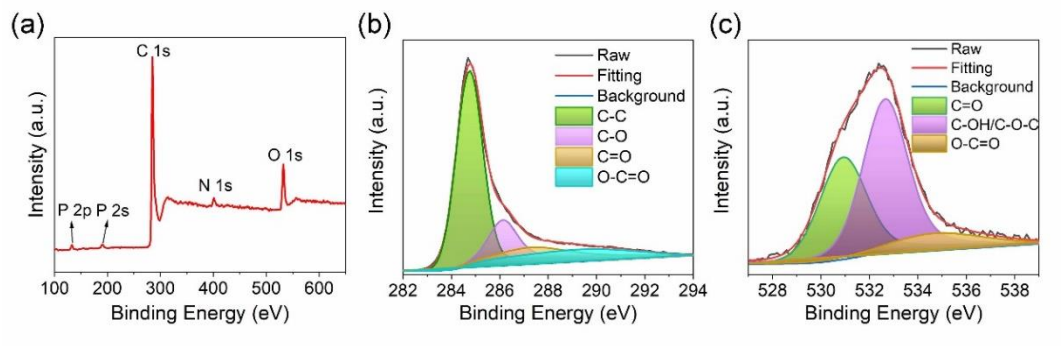

Supplementary Figure 4. (a) Full-scale XPS spectra of N/P-MC@RGO. (b) C1s and (c) O1s high-resolution XPS spectra of N/P-MC@RGO.

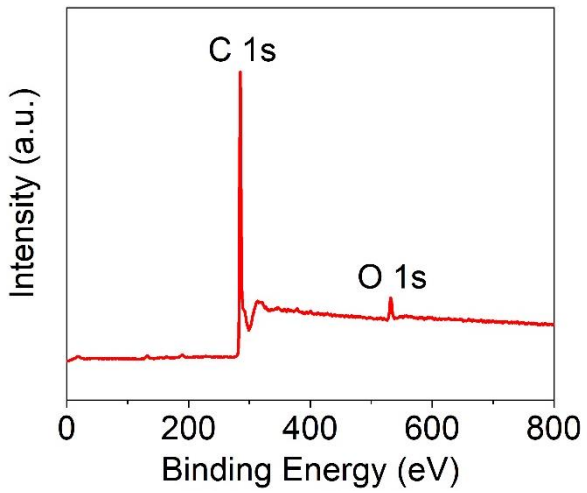

Supplementary Figure 5. (a) Full-scale XPS spectra of RGO.

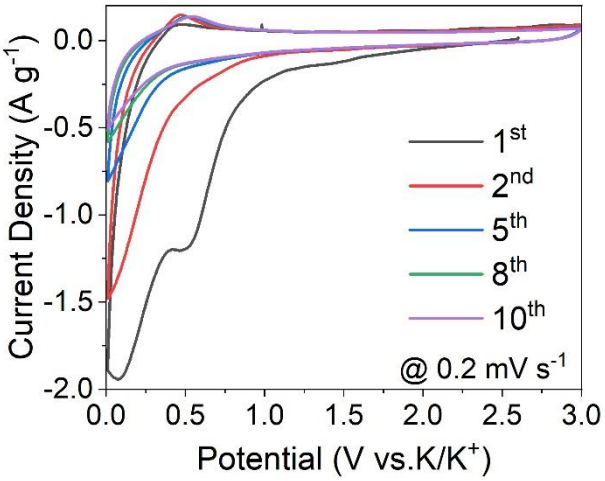

Supplementary Figure 6. The initial CV curves of N/P-MC@RGO anode at a sweep rate of 0.2 mV s^{-1}.

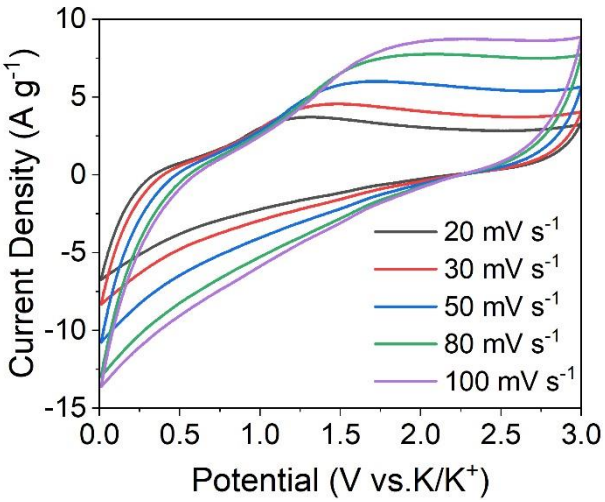

Supplementary Figure 7. The CV curves of N/P-MC@RGO anode with the scan rates from 20 mV s^{-1} to 100 mV s^{-1}.

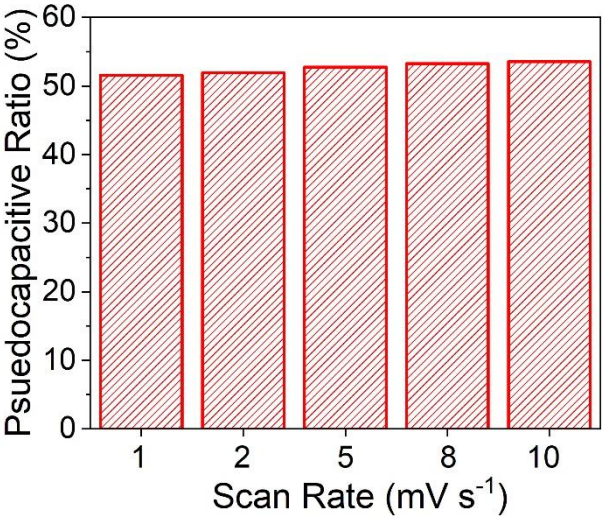

Supplementary Figure 8. Contribution ratio of the capacitive charge versus scan rate for N/P-MC@RGO anode.

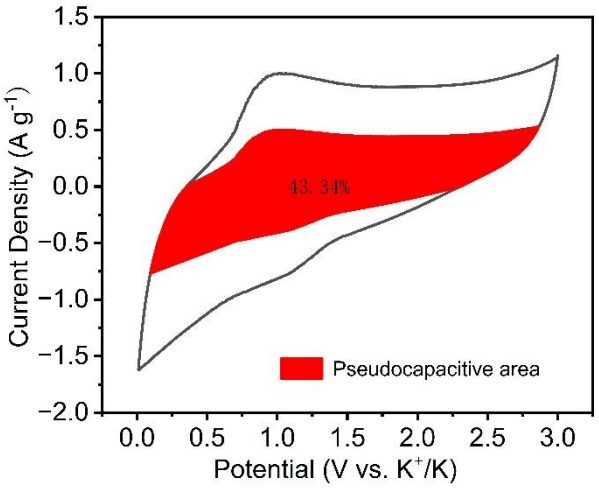

Supplementary Figure 9. Voltammetry response for N/P-MC electrode at 5 mV s^{-1}. The shaded region is associated to the capacitive contribution to the total current.

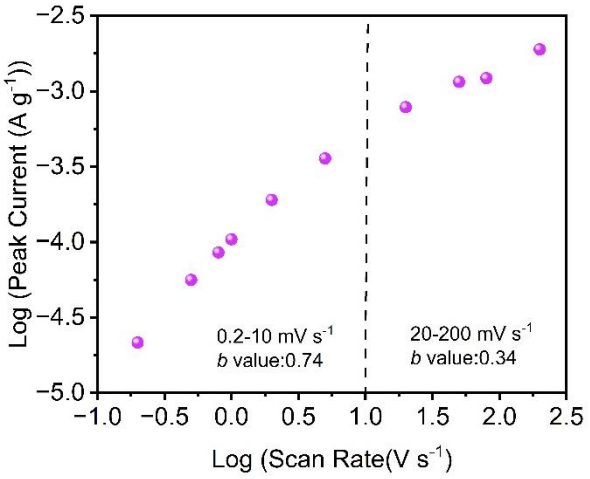

Supplementary Figure 10. *b* value evaluated from the anodic peak currents.

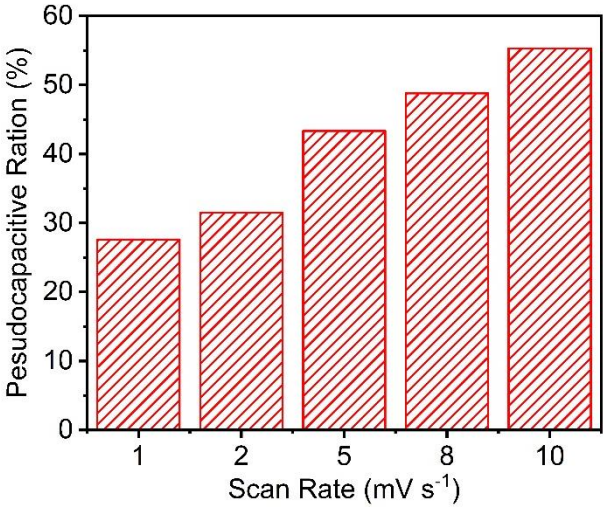

Supplementary Figure 11. Contribution ratio of the capacitive charge versus scan rate

for N/P-MC electrode.

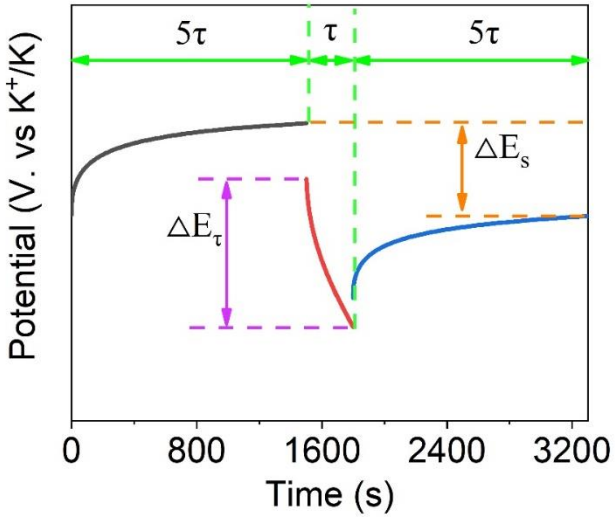

Supplementary Figure 12. Schematic illustration of essential parameters in GITT analysis during charging/discharging process.

GITT is considered as a powerful method to evaluate the apparent ion diffusion coefficient at different-equilibrium potentials. In this work, the charging/discharging current density is set to 0.1 A g^{-1} with a relatively short period of 300s (τ) to induce a potential shift ($\boldsymbol{\Delta}E_\tau$), followed by much longer relaxed period of 1500s to reach a quasi-equilibrium potential for the calculation of ($\boldsymbol{\Delta}E_s$). The titration-relaxation cycle is performed continuously at the potential window of 0.01-3.0 V vs. K/K^+. The apparent ion diffusion coefficient (D, $cm^2\ s^{-1}$) is calculated based on the following equation with sufficiently small current:

$$D = \frac{4}{\pi}\left(\frac{mV_m}{MA}\right)^2\left(\frac{\Delta E_S/\tau}{dE_t/d\sqrt{\tau}}\right)^2 = \frac{4}{\pi}L^2\left(\frac{\Delta E_S/\tau}{dE_t/d\sqrt{\tau}}\right)^2$$

Where m (g) is mass loading, Vm ($cm^3\ mol^{-1}$) is molar volume of the electrode, M (g mol-1) is molar weight of the electrode, A (cm^2) is electroactive area of the electrode, $\boldsymbol{\Delta}E_s$ (V) is the change of quasi-equilibrium potential after two sequential relaxation period, τ (s) is charge/discharge time during each titration, $dE\tau/d\sqrt{\tau}$ ($V\ s^{-1/2}$) is potential shift rate, and L (cm) is the thickness of the electrode. For an electrode-level analysis, the geometric area of the electrode is thus used as the electroactive area to highlight the significance of

porosity of the apparent K^+ diffusion. The above equation can be simplified by applying the small current density for a sufficiently short time in each titration, so that $dE\tau/d\sqrt{\tau}$ can be estimated as a stepwise constant for each titration:

$$D = \frac{4}{\pi} L^2 \left(\frac{\Delta E_S/\tau}{\Delta E_t/d\sqrt{\tau}}\right)^2 = \frac{4}{\pi} L^2 \left(\frac{\Delta E_S}{\tau \Delta E_t}\right)^2$$

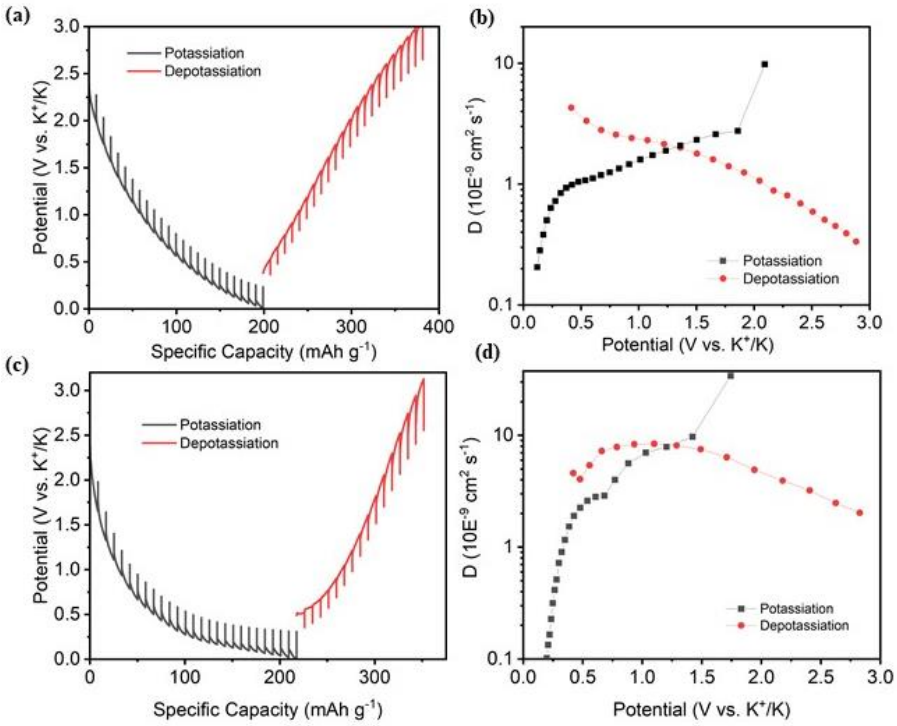

Supplementary Figure 13. (a) GITT test on N/P-MC anode. (b) The K^+ diffusion coefficient for N/P-MC evaluated by GITT method during the different charge/discharge process. (c) GITT test on RGO anode. (d) The K^+ diffusion coefficient for RGO evaluated by GITT method during the different charge/discharge process.

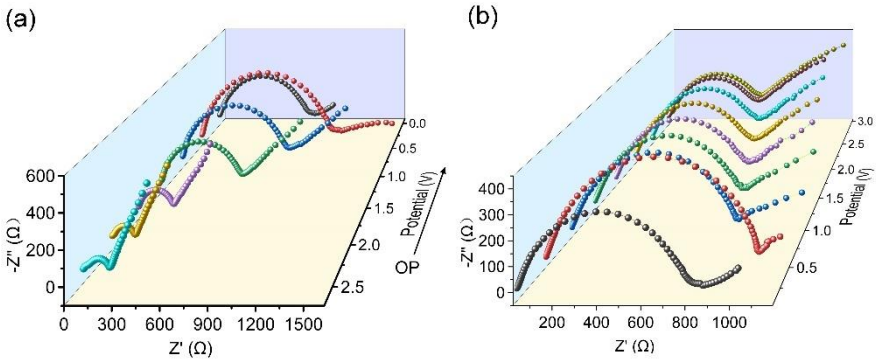

Supplementary Figure 14. EIS spectra of N/P-MC@RGO half cell achieved during the

(a) initial discharge and (b) charge processes.

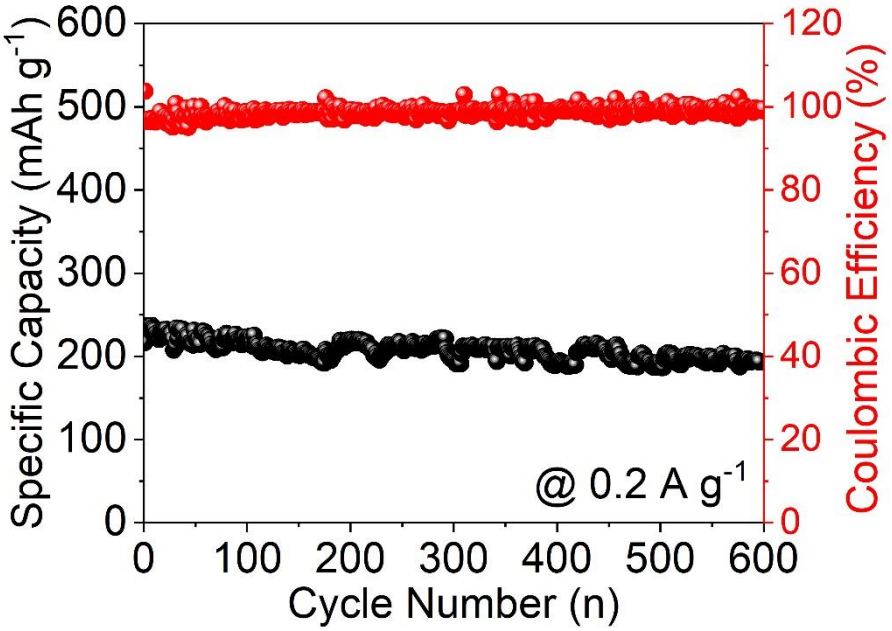

Supplementary Figure 15. Cycling performance of N/P-MC@RGO anode at 0.2 A g^{-1}.

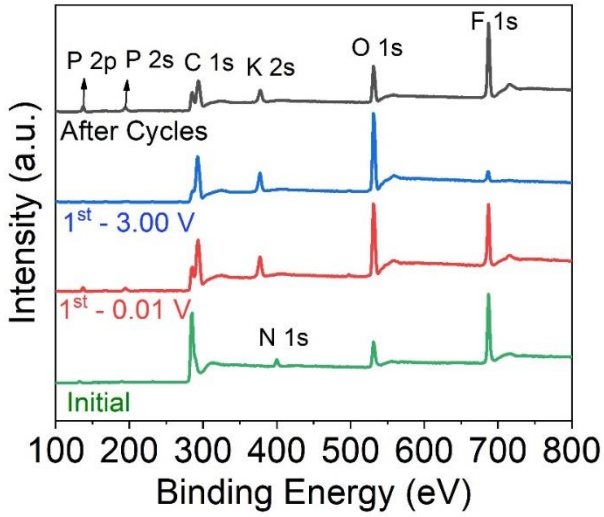

Supplementary Figure 16. Ex-situ XPS spectra curves of N/P-MC@RGO anode during the different charging/discharging states: pristine state (green), initial potassiated state (red), initial depotassiated state (blue), depotassiated state after long-term cycles (black).

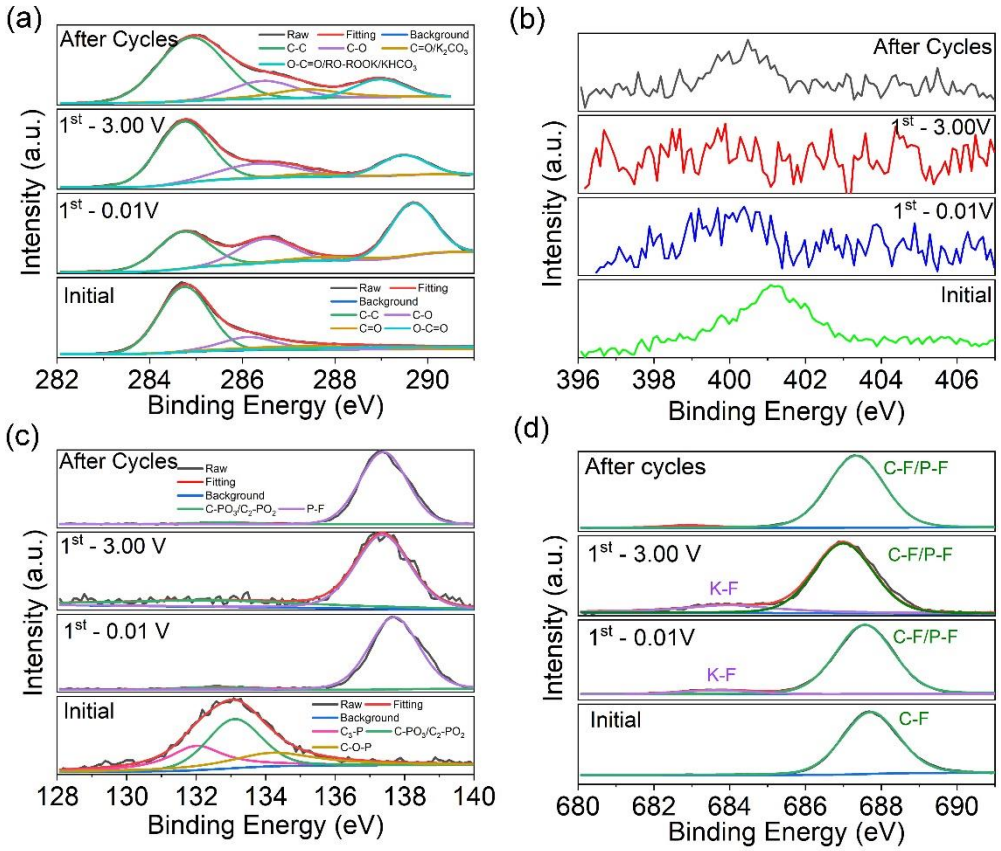

Supplementary Figure 17. High-resolution (a) C1s, (b) N1s, (c) P2p, and (d) F1s ex-situ XPS spectra curves of N/P-MC@RGO anode during the different charging/discharging states.

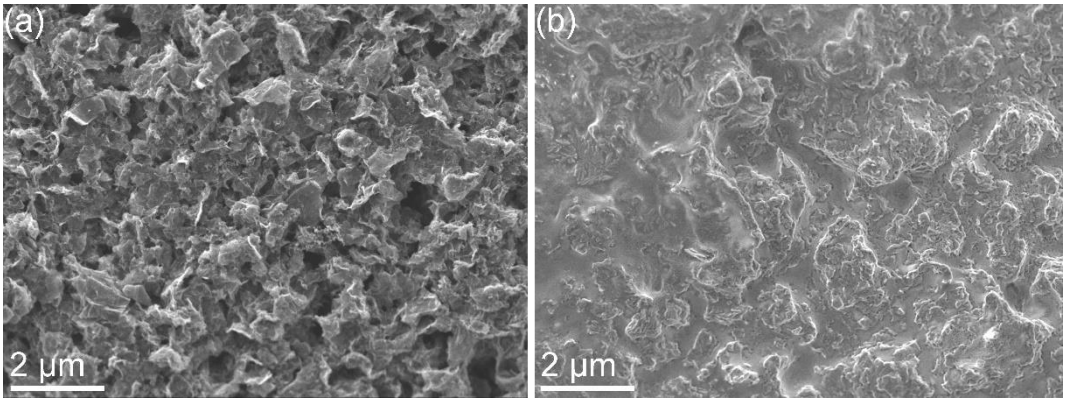

Supplementary Figure 18. SEM images of N/P-MC@RGO anode (a) before and (b) after long cycles.

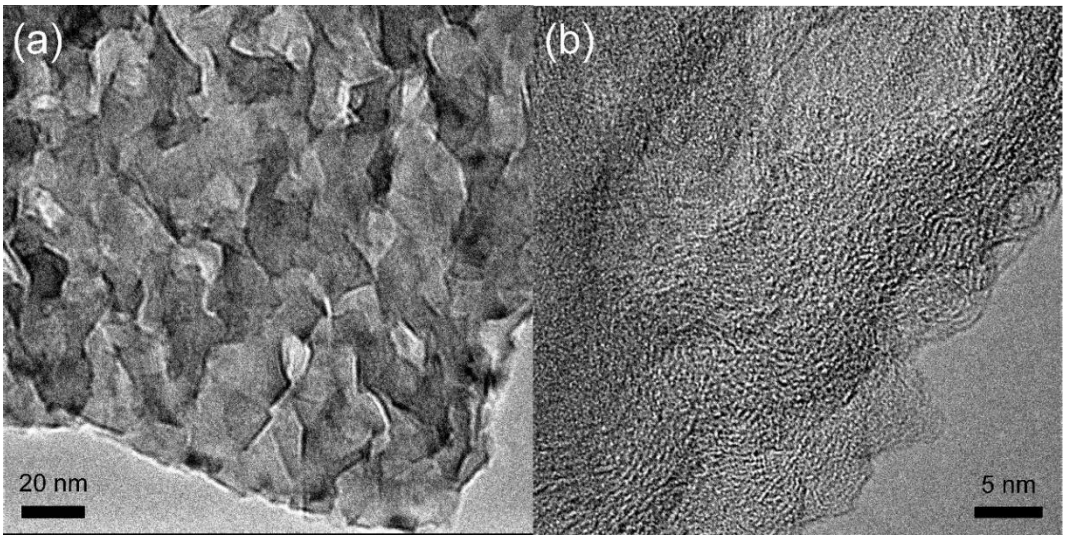

Supplementary Figure 19. (a) and (b) TEM images of N/P-MC@RGO after cycles.

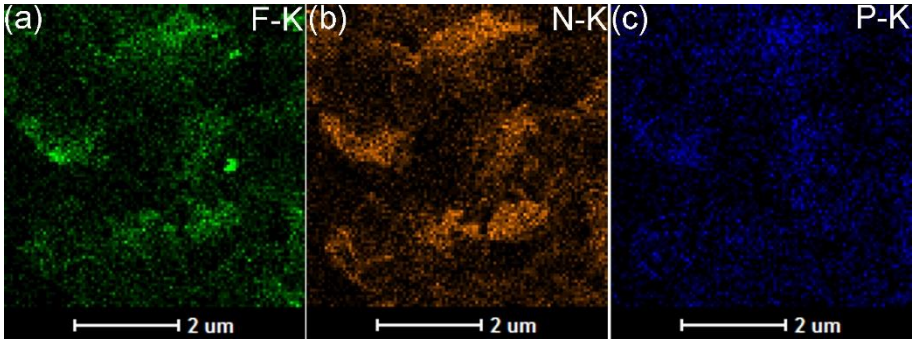

Supplementary Figure 20. Supplementary EDS mappings of (a) F, (b) N, and (c) P for N/P-MC@RGO after cycles.

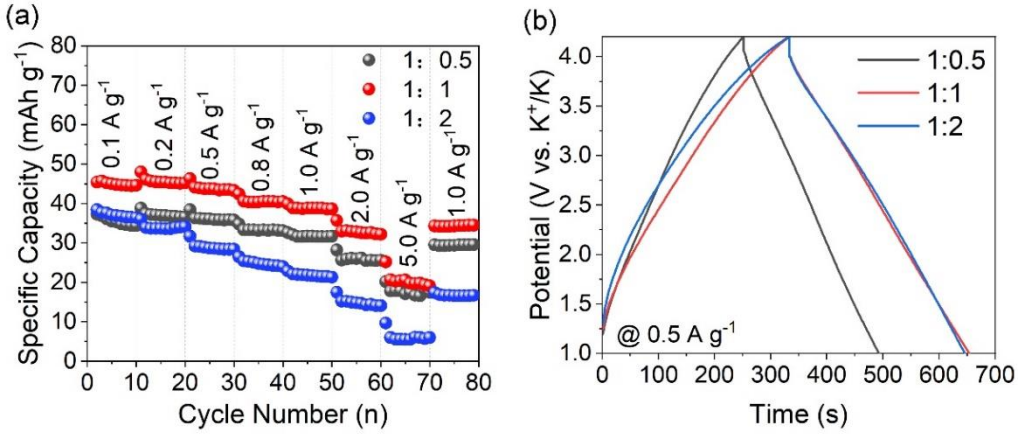

Supplementary Figure 21. The electrochemical performance of as-fabricated PICs with the different anode/cathode mass ratios: (a) rate capability from 0.1 to 5 A g^{-1}, (b)

charge/discharge curves at 0.5 A g^{-1}.

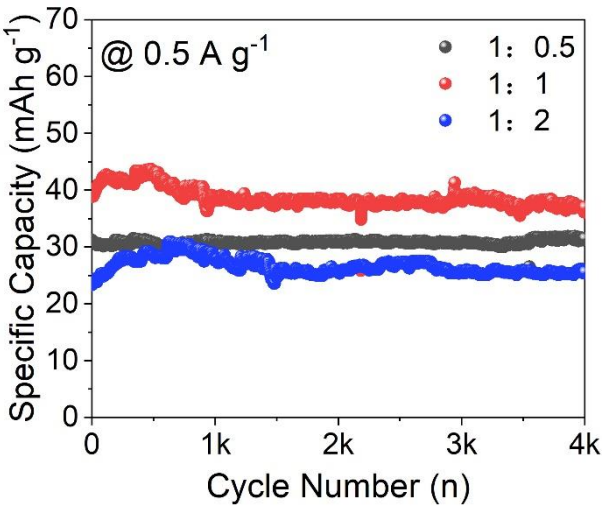

Supplementary Figure 22. Cycling performance at 0.5 A g^{-1} of as-fabricated PICs with the different anode/cathode mass ratios.

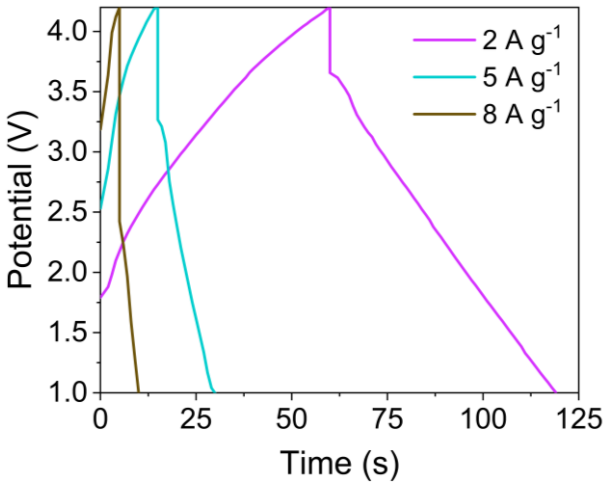

Supplementary Figure 23. Charge/discharging curves under the different current densities from 2 to 8 A g^{-1}.

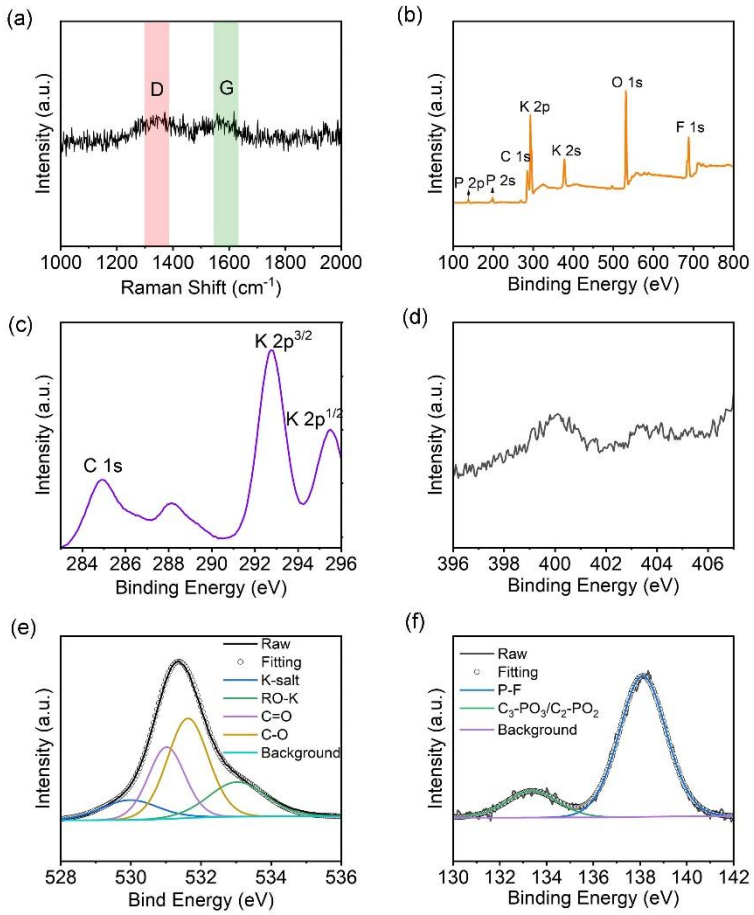

Supplementary Figure 24. Structural and surface information of N/P-MC@RGO anode detached from PICs after long-term cycles: (a) Raman spectra, (b) full-scale XPS, (c) C 1s XPS spectrum, (d) N 1s XPS spectrum, (e) O 1s XPS spectrum, and (f) P 2p XPS spectrum.

Supplementary Table 1. Physical Parameters for RGO, N/P-MC, N/P-MC@RGO samples

Sample	S_{BET}[a] ($m^2\ g^{-1}$)	S_{micro}[b] ($m^2\ g^{-1}$)	V_t[c] ($cm^3\ g^{-1}$)	D_{avg}[d] (nm)	I_D/I_G	C (at.%)	N (at.%)	O (at.%)	P (at.%)
N/P-MC@RGO	831.4	106.67	1.93	9.30	1.34	84.68	4.17	6.53	3.37
N/P-MC	1009.1	268.94	2.471	9.80	1.70	79.52	3.99	12.32	3.04
RGO	750.95	69.83	3.09	3.19	1.23	93.99	0.98	3.70	1.33

*a-BET surface area; b-BET surface area contributed by micropores; c-Total volume of pore; d-average pore width.

Supplementary Table 2. A summary of characteristic EIS data and the kinetic parameters of N/P-MC@RGO anode based half cell under the different cycles obtained from equivalent circuit model ($R_0(R_1Q_1)(R_2Q_2)Q_3$)

Cycle Numbr (n)	**Rs (R_0, Ω)**	**R_{SEI} (R_1, Ω)**	**R_{ct} (R_2, Ω)**	**CPE1-T ($S\cdot sec^n$)**	**CPE1-P (n)(0<n<1)**	**CPE2 -T ($S\cdot sec^n$)**	**CPE2-P (n)(0<n<1)**	**CPE3-T ($S\cdot sec^n$)**	**CPE3-P (n)(0<n**	**Chi-Squard**
Initial	6.135	6.624	425.4	4.77E-5	0.85	6.22E-5	0.86	0.0032	0.51	0.0022
200	11.51	11.66	537.6	5.36E-5	0.84	1.02E-4	0.78	0.0029	0.60	0.00091
400	15.62	18.64	600.1	7.64E-5	0.74	9.56E-5	0.77	0.0028	0.63	0.00067
600	18.69	26.45	652.4	9.61E-5	0.68	9.59E-5	0.75	0.0031	0.62	0.00053

Supplementary Table 3. Binding energy (B.E.) of K atom adsorption in different structure styles

Structure style	P-C	N5-C	N5/P-C	N6-C	N6/P-C	NQ-C	NQ/P-C
B.E. (eV)	-1.32	-2.96	-3.03	-2.62	-1.9	-0.89	-1.61

Supplementary Table 4. A summary of the kinetic parameters of N/P-MC@RGO//PDPC PIC and other typical carbon anode electrodes and other state-of-art PICs.

PICs type	Working Potential (V)	Energy Density (Wh kg^{-1})	Power Density (W kg^{-1})	Cycling Life	Ref
Graphite//AC	0-4	57.8	15,887	91% after 5,000 cycles at 15 A g^{-1}	54
Soft Carbon (SC) //AC	0-4	120	599	71.4% after 1,000 cycles at 0.35 A g^{-1}	52
N-Graphene//AC	0-3.0	51	9,600	80% after 10,000 cycles at 0.8 A g^{-1}	53
NHCS[a]//ANHCS[b]	0-4	114.2	8,203	80.4% after 5,000 cycles at 2 A g^{-1}	55
N/P-Graphene[c]//AC	1-4	195	1,4976	70% after 1,000 cycles at 1 A g^{-1}	56
NCNTs[d]//AC	0.01-4	117.1	1713.4	81.6% after 2000 cycles at 1 A g^{-1}	57
Hard Carbon (HC) //AC	0-3	77	2800	80% after 10,000 cycles at 0.8 A g^{-1}	58
N-CNTs[e]//LSG[f]	1-4	65	80	91.8% after 5,000 cycles at 0.4 A g^{-1}	59
MDPC[h]//PDPC[i]	1-4	120	26,000	79% after 120,000 cycles at 2 A g^{-1}	32
N/P-MC@RGO //PDPC	1-4.2	107	18,300	95.3% after 4,000 cycles at 0.5 A g^{-1}; 76.3% after 40,000 cycles at 2 A g^{-1}	Our Work

*a-Nitrogen-doped hierarchical porous hollow carbon spheres; b-Activated nitrogen-

doped hierarchical porous hollow carbon spheres; c-Nitrogen and phosphorus co-doped graphene; d-Hierarchical porous activated carbon; e-N-doped carbon nanotubes; f-nitrogen doped carbon nanotubes; g-three dimensional (3D) laser scribed graphene; h-Mn-MOF derived porous carbon; i-polyaniline derived porous carbon.